Thyroid Dysfunction Associated With Follicular Cell Steatosis in Obese Male Mice and Humans

Min Hee Lee,* Jung Uee Lee,* Kyong Hye Joung,* Yong Kyung Kim, Min Jeong Ryu, Seong Eun Lee, Soung Jung Kim, Hyo Kyun Chung, Min Jeong Choi, Joon Young Chang, Sang-Hee Lee, Gi Ryang Kweon, Hyun Jin Kim, Koon Soon Kim, Seong-Min Kim, Young Suk Jo, Jeongwon Park, Sheue-Yann Cheng, and Minho Shong

Research Center for Endocrine and Metabolic Diseases (M.H.L., K.H.J., Y.K.K., M.J.R., S.E.L., S.J.K., H.K.C., M.J.C., J.Y.C., H.J.K., K.S.K., Y.S.J., M.C.), Chungnam National University School of Medicine, Daejeon 301-721, Republic of Korea; Department of Pathology (J.U.L.), Daejeon St. Mary's Hospital, College of Medicine, The Catholic University of Korea, Daejeon 301-723, Republic of Korea; Department of Biomedical Science (S.-H.L.), Korea Advanced Institute of Biological Science, Daejeon 305-701, Korea; Department of Biochemistry (G.R.K.), Chungnam National University School of Medicine, Daejeon 301-721, Republic of Korea; Department of Nuclear Medicine (S.-M.K.), Chungnam National University and Hospital, Daejeon 301-721, Republic of Korea; and Laboratory of Molecular Biology (J.P., S.-Y.C.), National Cancer Institute, Bethesda, Maryland 20892

Adult thyroid dysfunction is a common endocrine disorder associated with an increased risk of cardiovascular disease and mortality. A recent epidemiologic study revealed a link between obesity and increased prevalence of hypothyroidism. It is conceivable that excessive adiposity in obesity might lead to expansion of the interfollicular adipose (IFA) depot or steatosis in thyroid follicular cells (thyroid steatosis, TS). In this study, we investigated the morphological and functional changes in thyroid glands of obese humans and animal models, diet-induced obese (DIO), *ob/ob*, and *db/db* mice. Expanded IFA depot and TS were observed in obese patients. Furthermore, DIO mice showed increased expression of lipogenesis-regulation genes, such as sterol regulatory element binding protein 1 (SREBP-1), peroxisome proliferator-activated receptor γ (PPARγ), acetyl coenzyme A carboxylase (ACC), and fatty acid synthetase (FASN) in the thyroid gland. Steatosis and ultrastructural changes, including distension of the endoplasmic reticulum (ER) and mitochondrial distortion in thyroid follicular cells, were uniformly observed in DIO mice and genetically obese mouse models, *ob/ob* and *db/db* mice. Obese mice displayed a variable degree of primary thyroid hypofunction, which was not corrected by PPARγ agonist administration. We propose that systemically increased adiposity is associated with characteristic IFA depots and TS and may cause or influence the development of primary thyroid failure. **(*Endocrinology* 156: 1181–1193, 2015)**

Intracellular lipids are required for the maintenance of cellular structural integrity and energy homeostasis (1, 2). However, excessive accumulation of lipids, particularly triglycerides (TG), causes steatosis within nonadipose tissues (3). Steatosis is associated with multiple factors including excessive synthesis and defective elimination of TGs, which may lead to lipid droplet formation in the cytoplasm (4). Obesity is the most common cause of steatosis in the liver, muscle, kidney, heart, and endocrine beta cells (5). Steatosis associated with lipid droplets is well characterized in the liver but it is not fully understood in other tissues (6). It has been suggested that steatosis causes cellular dysfunction in nonadipose tissue in patients with obesity (7).

ISSN Print 0013-7227 ISSN Online 1945-7170
Printed in U.S.A.

Received August 10, 2014. Accepted December 22, 2014.
First Published Online January 2, 2015

* M.H.L., J.U.L., and K.H.J. contributed equally to the study.

Abbreviations: ACC, acetyl coenzyme A carboxylase; BMI, body mass index; DIO, diet-induced obese; EM, electron microscope; ER, endoplasmic reticulum; FASN, fatty acid synthetase; HFD, high fat diet; IFA, interfollicular adipose; NCD, normal-chow diet; PPAR, peroxisome proliferator-activated receptor; RGZ, rosiglitazone; SREBP-1, sterol regulatory element binding protein-1; TG, triglyceride; TS, thyroid steatosis.

Adult thyroid dysfunction, which is one of the most common endocrine dysfunctions, is associated with an increased risk of cardiovascular mortality (8). In a recent epidemiologic study, obesity was linked to many endocrine abnormalities including thyroid abnormalities (9, 10). The prevalence of hypothyroidism was higher in obese patients than in a control group of age- and sex-matched subjects with a normal body mass index (BMI) (11). The underlying mechanism of the association between obesity and thyroid dysfunction is largely unknown. A recent study demonstrated that obese mice may experience thyroid dysregulation as a result of changes in the hypothalamus-pituitary-thyroid axis (12). Taken together, these data definitely suggest that endocrine factors, including leptin, which are dysregulated in excessive adiposity, are important etiological factors leading to a dysregulated hypothalamus-pituitary-thyroid axis in obese individuals.

Endocrine organs are also affected by steatosis, and endocrine dysfunction in patients with obesity may be caused by steatosis (13). In obesity, excessive accumulation of lipids in pancreatic beta cells causes progressive beta cell dysfunction (14, 15), resulting in early type 2 diabetes and ultimately insulin-dependent diabetes (7, 16, 17).

Unlike pancreatic beta cells, the thyroid gland contains a small amount of adipose depots that may give rise to abnormal adipose tissue lesions, such as lipomatosis (18), liposarcoma (19), and a heterotopic nest of adipocytes (20). However, intrathyriodal adipocytes have not been regarded as an important regulator of thyroid function. It is also unclear whether adipocytes in the thyroid gland expand as a consequence of increased adiposity in obesity. Adipocytes secrete paracrine factors that may regulate thyroid function, and steatosis in thyroid follicular cells (thyroid steatosis, TS) may alter the thyroid endocrine function (21, 22). It is conceivable that excessive adiposity during obesity might result in expansion of the interfollicular adipose (IFA) depot or TS.

In this study, we demonstrated the presence of IFA depot and TS in the thyroid gland of patients with obesity. In addition, we used male mouse models of obesity, such as diet-induced obese (DIO), *ob/ob,* and *db/db* mice to investigate the relevant morphological and functional changes in the thyroid gland. We found intracellular lipid droplets in follicular cells, which we suggest may cause thyroid dysfunction in obese mouse models.

Materials and Methods

Subjects

We examined the contralateral lobe of the thyroid in 35 patients with papillary microcarcinoma to observe IFA depots and TS. We examined the thyroid tissue in patients with normal adiposity (BMI < 25), obesity ($25 \leq$ BMI < 30), and severe obesity (BMI ≥ 30) for the presence of IFA depots and TS.

Animals

All mice used in this study were male. The genetically obese mice (*ob/ob*, *db/db*, and the C57BL/6J strain) and age-matched controls were purchased from the Jackson Laboratory. For the high-fat diet (HFD; 60% of calories came from fat) time course experiments, 6-week-old mice were subjected to HFD feeding for 8 and 16 weeks. All animal experiments were approved by the Institutional Animal Care and Use Committee of the Chungnam National University School of Medicine (approval ID, CNU-00246).

Histological and immunohistochemical analysis

Horizontal sections of the formalin-fixed thyroid tissue were taken serially in a superior-to-inferior direction (0.5 cm thickness). The tissue blocks, which contained two serial sections of the upper pole, two serial sections of the mid pole, and two serial sections of the lower pole, were embedded in paraffin, then cut in a microtome (4 μm thickness). Each paraffin-embedded tissue section was stained with hematoxylin and eosin (H&E). The areas of IFA depots were calculated in six representative sections of the thyroid gland from nine patients with a BMI less than 25. The mean area of IFA depot was 0.11 with a standard deviation of 0.10. We have calculated the reference range (95% confidence interval) of the percentage of IFA depots showing an upper limit of 0.19. We classified patients showing an IFA of less than 0.19 as IFA (−). The data are presented as percentage values in Supplemental Figure 1A [IFA (−) vs IFA (+) group; $0.04 \pm 0.03\%$ vs $0.45 \pm 0.20\%$, $P < .001$].

To evaluate TS, we calculated the number of thyroid follicular cells showing severe ballooning degeneration and discrete lipid droplets in 50 follicles on each slide out of a total of six slides from each patient. The follicles on each slide were randomly selected at the periphery and center of the slides by two investigators independently. The follicular cells containing lipid droplets were expressed as TS (+) cells/follicle area (mm^2). The thyroid gland obtained from nonobese (BMI < 25) IFA (−) patients showed less than 10 lipid droplet–containing cells/follicle area (mm^2). We defined the TS (+) group arbitrarily as those having more than 100 lipid droplet–containing cells/follicle area (mm^2).

The genetically obese mice (*ob/ob*, *db/db*, and the C57BL/6J strain) and the age- and sex-matched controls fed on a normal-chow diet (NCD) or HFD for 8 or 16 weeks were killed and their thyroid glands excised. Paraffin sections were prepared and stained with H&E. At least five sections from each mouse were used for image inside analysis. Immunohistochemistry staining for sterol regulatory element binding protein-1 (SREBP-1) and thyroglobulin was performed in the thyroid tissue of NCD- and HFD-fed mice. Tissue sections were then incubated for 60 minutes at room temperature (at 23°C), with the following primary antibodies: SREPB-1 rabbit mAb, thyroglobulin mouse mAb (Santa Cruz Biotechnology, Inc). Immunohistochemistry was performed using a Polink-1 HRP Rat-NM 3,3′-diaminobenzidine Detection System (GBI, Inc).

Immunofluorescence staining

Thyroid tissues were isolated from *ob*/+, *ob*/*ob*, *db*/+, and *db*/*db* mice at 6 and 13 weeks of age, and cryostat sections (4 μm) were collected on glass slides and fixed in 3.7% paraformaldehyde. Sections were blocked for 2 hours in 5% BSA in PBS, and incubated with the primary antibodies, β-catenin (1:200, Santa Cruz) and the fluorescent dye, BODIPY (1:100, Molecular Probes) overnight at 4°C. The stained slides were observed using an Olympus Fluoview FV1000 microscope equipped with a charge-coupled device camera (Olympus Corp).

Transmission electron microscopy analysis

The thyroid tissues were fixed in 2.5% glutaraldehyde in 0.1M cacodylate buffer at 4°C for 4 hours. After washing in 0.1M cacodylate, samples were postfixed in 1% OsO_4 in cacodylate buffer (pH 7.2) containing 0.1% $CaCl_2$ for 1 hour at 4°C. Samples were analyzed with an electron microscope (EM) (Tecnai G2 Spirit Twin; FEI Company; Korea Basic Science Institute).

RNA extraction and real-time qRT-PCR analysis

RNA was isolated using TRIzol (Invitrogen). cDNA was synthesized from 1 μg total RNA with M-MLV reverse transcriptase and oligo-dT primers according to the manufacturer's protocol. The PCR primers are shown in Supplemental Table 1. The results were normalized with 18s rRNA.

Serum analysis of hormones

Serum TSH concentrations were evaluated using a specific mouse TSH RIA provided by S.Y. Cheng (Center for Cancer Research, National Cancer Institute, Bethesda, MD). Intra-assay coefficient of variation was 5.88% and interassay coefficient of variation was 6.66%. Serum levels of hormones were measured using an ELISA kit (Leptin; EMD Millipore, T_3, T_4; Merck Millipore, Thyroglobulin; Cusabio Biotech Co Ltd) according to the manufacturer's instructions.

ELISA assay

TG and total cholesterol concentrations in the thyroid were measured using a TG quantification kit (Abcam) and a total cholesterol kit (Cell Biolab, Inc), respectively. Intrathyroidal T_3, T_4, and thyroglobulin levels were measured using Multi Species Steroid/Thyroid Hormone (T_3, T_4; Merck Millipore Corp) and a thyroglobulin ELISA kit (Cusabio Biotech Co Ltd).

Intraperitoneal glucose tolerance and insulin tolerance tests

For intraperitoneal glucose tolerance, mice were fasted overnight (16 hours) and then injected ip with 2 g/kg glucose. Fasting blood glucose levels were measured at 0, 5, 15, 30, 60, 90, and 120 minutes after the glucose injection with a glucometer (Accu-check, Hoffmann-La Roche Ltd). For insulin tolerance tests, mice were fasted for 6 hours and then injected ip with insulin (0.75 U/kg; Humalog, Eli Lilly Co) and blood glucose levels were measured with a glucometer (Accu-Chek, Hoffmann-La Roche Ltd).

Materials

Rosiglitazone (RGZ) was purchased from Sigma-Aldrich. MILLIPLEX MAP multi species Steroid/Thyroid Hormone Magnetic Bead Panel kit was purchased from Merck Millipore Corp. to measure the thyroid hormone levels. The following antibodies were used: β-catenin, SREBP-1, and thyroglobulin (Santa Cruz Biotechnology). The following fluorescent dyes were used: BODIPY (Life Technologies Co), and DAPI (Sigma-Aldrich Co).

Statistical analysis

Group comparisons of categorical variables were evaluated using the linear-by-linear association. The means were compared with the independent sample *t* test, one-way ANOVA, or the Mann-Whitney *U* test. Values are presented as the mean ± SD. $P < .05$ was considered statistically significant. Analyses were performed using SPSS Version 18.0 statistical software (SPSS Inc).

Results

Detection of intrathyroidal adipose tissue and lipid droplets in thyroid gland of obese subjects

To observe adipose depots and steatosis, we examined the thyroid tissue in patients with normal adiposity (BMI < 25), obesity ($25 \leq$ BMI < 30), and severe obesity (BMI ≥ 30) for the presence of IFA depots and TS (Figure 1, A–D). IFA were observed in the thyroid lobe of four of nine patients with BMI < 25 (Figure 1E). Interestingly, the frequency and area of adipose depot was significantly higher in the thyroid tissue of patients with BMI of at least 25 (detected in 19 of 26 patients) (Figure 1E).

TS was uncommon and was detected in only two of nine patients with BMI < 25 regardless of the presence of focal adipose tissue (Figure 1, D and E). Notably, a higher proportion of lipid droplets was frequently observed in patients with BMI of at least 25 (16 of 26 patients) (Figure 1, C–E). The simultaneous presence of IFA and TS was found in two of nine patients with BMI < 25 and in 13 of 26 patients with BMI of at least 25.

As shown in Supplemental Figure 1, B and C, serum free T_4 (BMI < 25 vs BMI ≥ 25; 1.1 ± 0.1 ng/dL vs 1.1 ± 0.1 ng/dL) and TSH levels (2.1 ± 1.3 μU/mL vs 2.3 ± 1.3 μU/mL) of obese patients (BMI ≥ 25) were not significantly different from those of nonobese (BMI < 25) patients. However, TSH levels were significantly higher in patient groups with IFA (+) and TS (+) than in patients with IFA (−) and TS (−) (IFA (−) TS (−) vs IFA (+) TS (+); 1.6 ± 1.3 μU/mL vs 2.7 ± 1.5 μU/mL, $P < .03$) (Figure 1F). A similar higher level of TSH was also noted in specific subgroups with TS (+) (TS (−) vs TS (+); 1.9 ± 1.2 μU/mL vs 2.6 ± 1.3 μU/mL, $P < .03$) (Supplemental Figure 1E). These findings suggested that ectopic fat accumulation, particularly steatosis of thyroid follicular cells, may result in primary hypothyroidism in obese patients.

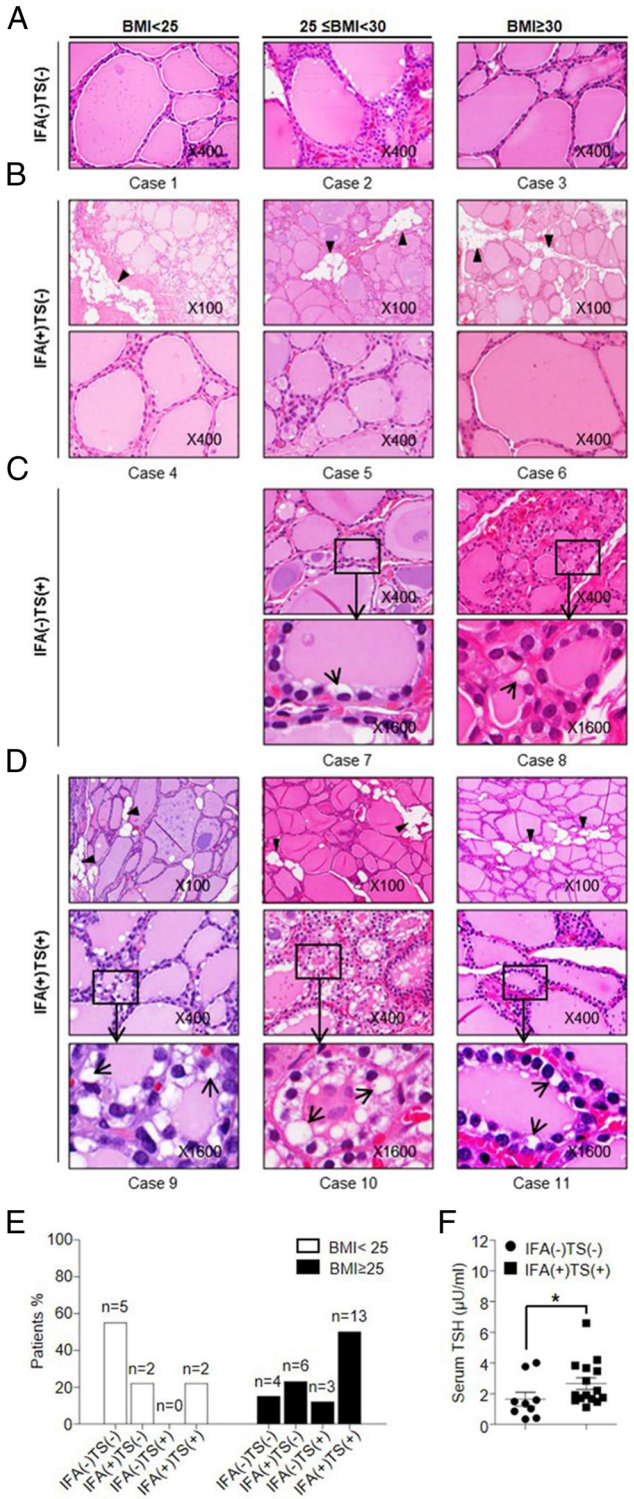

Figure 1. Interfollicular adipocytes and TS. A–D, Hematoxylin/eosin (H&E) staining showing thyroid follicles lined by flat or cuboidal thyroid follicular cells with interfollicular stromal infiltration by mature adipose tissue (arrowhead indicates IFA). Thyroid follicular cells displayed intracellular lipid droplets (TS). Large lipid droplets displaced the cytoplasm and distorted the nucleus (arrow). All images are shown at 100×, 400×, and 1600× magnification. E, IFA (−) and TS (−) were found in 55% (five of nine cases) of patients with a BMI < 25, compared with 15.4% (four of 26 cases) in those with BMI ≥ 25. IFA (+) and TS (−) were found in 22.2% (two of nine cases) of patients with a BMI < 25, compared with 23.1% (six of 26 cases) in those with BMI ≥ 25. IFA (−) and TS (+) were not detected in patients with a BMI < 25, but were detected in 11.5% (three of 26 cases) of patients with a BMI ≥ 25. IFA (+) and TS (+) were present in 22.2% (two of nine cases) of patients with a BMI < 25, compared with 50% (13 of 26 cases) of patients with a BMI ≥ 25. F, TSH levels were measured in IFA (−) and TS (−) groups (n = 9) and IFA (+) and TS (+) group (n = 15).

Taken together, these findings suggest that focal adipose tissue in the thyroid gland is common and that it may expand with increasing systemic adiposity. Indeed, follicular cell steatosis was closely associated with increased systemic adiposity.

Thyroid dysfunction in HFD-fed mice

Next, we investigated thyroid dysfunction in male mice (C57BL/6J) fed NCD or HFD for 8 weeks. Body weight increased significantly in DIO, HFD-fed mice compared with lean NCD-fed mice (Figure 2A). The tissue weight between lean and DIO mice was different only in epididymal white adipose tissue and brown adipose tissue; however, the tissue-weight-to-body-weight ratio was significantly higher in muscle as well as epididymal white adipose tissue and brown adipose tissue of DIO mice than in lean mice (Supplemental Figure 2, A and B). The thyroid weight did not differ between lean mice and DIO mice (NCD-fed vs HFD-fed mice; 9.6 ± 0.2 mg vs 9.3 ± 0.5 mg), but the thyroid-weight-to-body-weight ratio was significantly lower in DIO mice (NCD-fed vs HFD-fed mice; 1 ± 0.1 vs 0.7 ± 0.06, $P < .002$) (Figure 2, B and C).

DIO mice showed lower serum T_3 (NCD-fed vs HFD-fed mice; 0.44 ± 0.08 ng/mL vs 0.34 ± 0.07 ng/mL, $P < .004$) and T_4 levels (NCD-fed vs HFD-fed mice; 3.64 ± 0.37 μg/dL vs 3.23 ± 0.3 μg/dL, $P < .026$) (Figure 2, D and F). The intrathyroidal concentration of T_3 (NCD-fed vs HFD-fed mice; 8 ± 0.7 pg/ng vs 6.5 ± 0.6 pg/ng, $P < .015$) and T_4 (NCD-fed vs HFD-fed mice; 53.6 ± 3.3 pg/ng vs 42.0 ± 4.3 pg/ng, $P < .021$) was significantly lower in DIO mice (Figure 2, E and G). Serum TSH levels in DIO mice were higher than in lean mice (NCD-fed vs HFD-fed mice; 36 ± 9 ng/mL vs 65.8 ± 7.2 ng/mL, $P < .001$) (Figure 2H). As expected, the serum leptin level in DIO mice was markedly higher (Supplemental Figure 2C). Taken together, these findings suggest that DIO mice have primary thyroid dysfunction, which increases TSH secretion in the pituitary gland.

To examine the expression pattern of genes involved in thyroid hormone production in response to TSH, we analyzed thyroid-specific mRNAs known to be regulated by TSH. The expression of TSH receptor, thyroperoxidase, sodium-iodide symporter, and thyroglobulin was higher

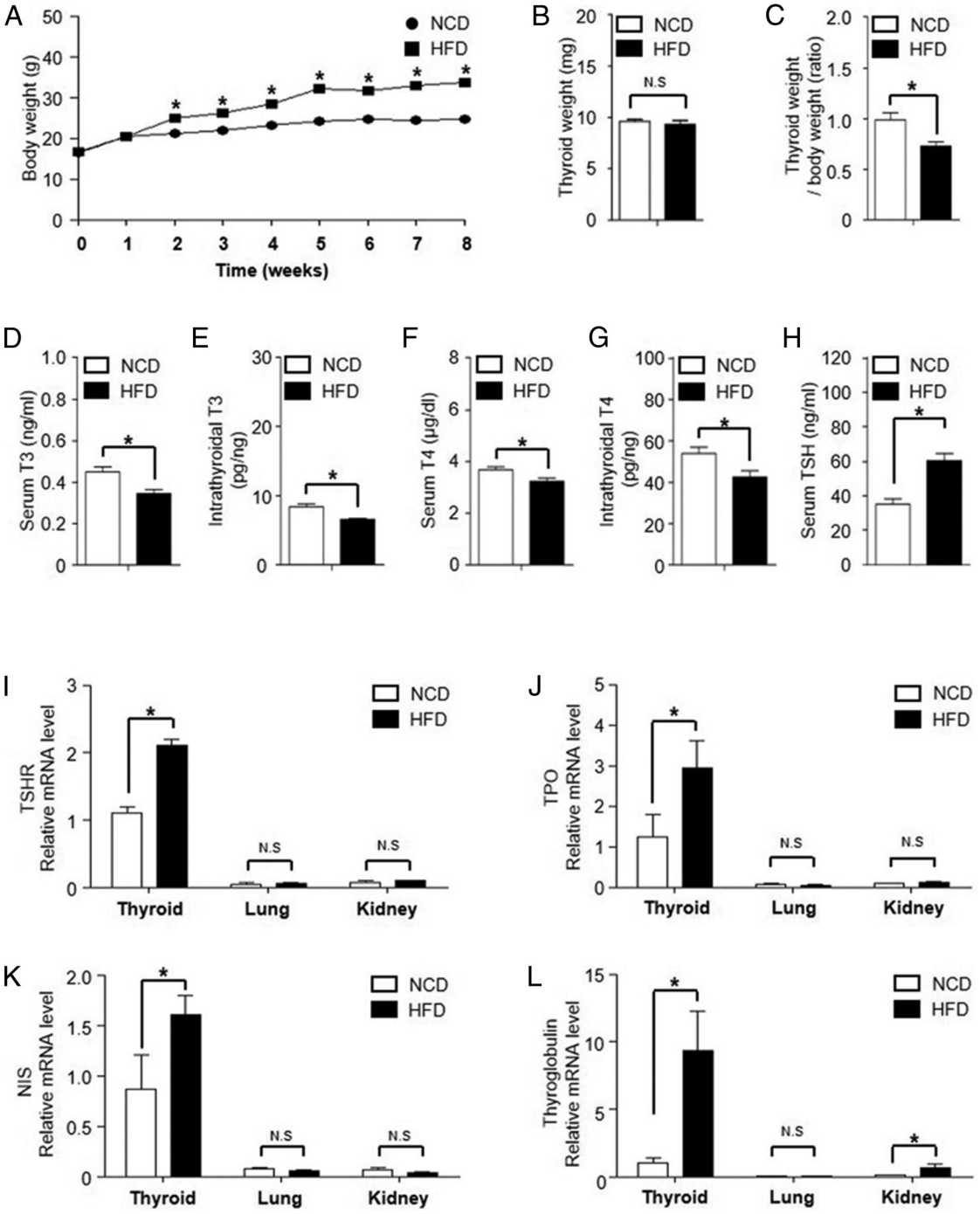

Figure 2. Thyroid function in mice with diet-induced obesity. Six-week-old male C57BL/6J mice were fed NCD or HFD, and their weights were monitored for 8 weeks until 14 weeks of age. A, Body weight of NCD- (filled circle) or HFD-fed (filled square) mice (n = 10 per group). B and C, The thyroid weight (B) and the thyroid-weight-to-body-weight ratio (C) were measured in NCD- (open bars) or HFD-fed (filled bars) mice as indicated (n = 10 per group). D–H, Serum T_3 (D), T_4 (F), and TSH (H) levels (n = 40 per group), and intrathyroidal T_3 (E) and T_4 (G) levels (n = 8 per group). Levels were measured in NCD- and HFD-fed mice. I–L, RT-qPCR analysis of relative gene expression of TSH receptor (TSHR), thyroperoxidase (TPO), sodium-iodide symporter (NIS), or thyroglobulin (Tg) was carried out in the thyroid, lung, and kidney of NCD- or HFD-fed mice for 8 weeks. mRNA was normalized to the expression of 18S rRNA. Values are means ± SD; *, $P < .05$; N.S., not significant.

in the thyroid gland of DIO mice (Figure 2, I–L). The thyroglobulin content was lower in the DIO mice than in lean mice (Supplemental Figure 2, D and E). These findings suggest that DIO mice have primary thyroid dysfunction characterized by high serum TSH levels.

Lipogenesis and steatosis in thyroid follicular cell in DIO mice

To investigate whether TS is associated with lipogenesis, we performed histological and molecular biological analyses of the thyroid gland in DIO mice. Lipid droplets

in thyroid follicular cells were not observed in the thyroid tissue of lean mice (Figure 3A). However, thyroid follicular cells in the central follicle of the thyroid tissue in DIO, HFD-fed mice for 8 and 16 weeks frequently contained lipid droplets. (Figure 3A and Supplemental Figure 3A). IFA depots were significantly higher in all DIO, HFD-fed mice for 8 (NCD-fed vs HFD-fed mice; 12.8 ± 3.4% vs 24.8 ± 10.7%, $P < .006$) (Figure 3B) and 16 weeks (NCD-fed vs HFD-fed mice; 5.4 ± 0.76% vs 30.8 ± 0.77%, $P < .003$) (Supplemental Figure 3B). Furthermore, using transmission EM, we found that thyroid follicular cells in DIO mice had a luminal swelling in the endoplasmic reticulum (ER) (Supplemental Figure 3C). Serum TSH levels positively correlated with the area of IFA depots (%) (Pearson correlation coefficiency $r = 0.469$, $P < .04$). (Figure 3C). Consistently, DIO mice showed higher TG (NCD-fed vs HFD-fed mice; 10.7 ± 3.5 mg/mL vs 22.12 ± 4 mg/mL, $P < .029$) and cholesterol levels (NCD-fed vs HFD-fed mice; 58.5 ± 0.25 mg/mL vs 74 ± 2 mg/mL, $P < .029$) in thyroid than lean mice (Figure 3, D and E). TG and total cholesterol levels in the liver were significantly higher in DIO mice than in lean mice, whereas the levels in the lung did not differ between the two groups (Supplemental Figure 3, D and E). Endogenous SREBP-1 staining was barely detectable in the thyroid tissue of lean mice, but it was significantly up-regulated in the thyroid tissue of DIO mice (Figure 3J). Given that sterol regulatory element binding protein 1 (SREBP-1)-mediated lipogenesis may be a critical contributor to ectopic steatosis in obese mice and humans (23, 24), we investigated the changes in lipogenic genes expression in various tissues. The lipogenesis-regulating genes, such as peroxisome proliferator-activated receptor-γ (PPARγ), acetyl coenzyme A carboxylase (ACC), fatty acid synthetase (FASN), and SREBP-1 were up-regulated in the thyroid gland of DIO mice (Figure 3, F–I). Taken together, these results suggest that TG accumulated in thyroid gland, which, together with the induction of lipogenic genes, mediated fat accumulation in the liver and muscle of DIO mice.

Thyroid dysfunction in *ob/ob* and *db/db* mice

We investigated the features of steatosis in the thyroid gland of genetically obese mouse models, namely *ob/ob* and *db/db* mice, which have a more severe form of fat accumulation than DIO mice. In *ob/ob* mice, body weight was significantly higher than that of the control mice (Figure 4A). In particular, the thyroid weight (*ob/+* vs *ob/ob*; 7.6 ± 0.12 mg vs 5.9 ± 0.47 mg, $P < .001$) and the thyroid-weight-to-body-weight ratio (*ob/+* vs *ob/ob*; 1 ± 0.04 vs 0.6 ± 0.04, $P < .001$) were significantly lower in *ob/ob* mice than in *ob/+* mice (Figure 4, B and C; Supplemental Figure 4, A and B). To confirm these findings, we measured the specific gravity of thyroid tissues. The specific gravity of dissected thyroid tissues was significantly lower in *ob/ob* mice than in *ob/+* mice (Figure 4D). Serum T_3 (*ob/+* vs *ob/ob*; 0.24 ± 0.04 ng/mL vs 0.13 ± 0.02 ng/mL, $P < .014$) and T_4 (*ob/+* vs *ob/ob*; 4.17 ± 0.24 μg/dL vs 3.04 ± 0.14 μg/dL, $P < .002$) levels were significantly lower in *ob/ob* mice than in *ob/+* mice (Figure 4, E and G). Intrathyroidal T_3 (*ob/+* vs *ob/ob*; 14.2 ± 0.8 pg/ng vs 5.4 ± 1.0 pg/ng, $P < .001$) and T_4 (*ob/+* vs *ob/ob*; 134.5 ± 8.0 pg/ng vs 74.8 ± 6.0 pg/ng, $P < .001$) levels were significantly lower in ob/ob mice than in ob/+ mice (Figure 4, F and H). Serum TSH in *ob/ob* mice were consistently higher than in *ob/+* mice (*ob/+* vs *ob/ob*: 15.92 ± 2 ng/mL vs 24.24 ± 3.7 ng/mL, $P < .043$) (Figure 4I and Supplemental Figure 4C). In *db/db* mice, the body weight was significantly higher, and the thyroid weight (*db/+* vs *db/db*; 7.7 ± 0.2 mg vs 5.8 ± 0.42 mg, $P < .001$) and the thyroid-weight-to-body-weight ratio (*db/+* vs *db/db*; 1 ± 0.1 vs 0.5 ± 0.03, $P < .001$) were significantly lower in *ob/ob* mice than in *db/+* mice (Figure 4, J–L and Supplemental Figure 4, D and E). The specific gravity of the thyroid tissue of *db/db* mice was significantly lower than that of *db/+* mice (Figure 4M). Similarly to *ob/ob* mice, *db/db* mice also showed lower serum T_3 (*db/+* vs *db/db*; 0.27 ± 0.04 ng/mL vs 0.15 ± 0.04 ng/mL, $P < .031$) and T_4 (*db/+* vs *db/db*; 3.2 ± 0.4 μg/dL vs 2.24 ± 0.4 μg/dL, $P < .038$) levels than *db/+* mice (Figure 4, N and P). In addition, intrathyroidal T_3 (*db/+* vs *db/db*; 23.3 ± 6.0 pg/ng vs 16.0 ± 0.6 pg/ng, $P < .043$) and T_4 (*db*; 256.8 ± 50.0 pg/ng vs 179.6 ± 6.0 pg/ng, $P < .043$) levels were significantly lower in *db/db* mice than in *db/+* mice (Figure 4, O and Q). Consistently, the serum TSH level was higher at 118 ± 10 ng/mL ($P < .009$) in *db/db* mice than in *db/+* mice (*db/+* vs *db/db*: 31 ± 9.1 ng/mL vs 150.13 ± 16.3 ng/mL, $P < .016$) (Figure 4R and Supplemental Figure 4F). Collectively, these findings suggest that the thyroid gland has a lower weight in genetic mouse models of obesity, and primary thyroid dysfunction is present in *ob/ob, db/db,* and DIO mice.

Thyroid steatosis in *ob/ob* and *db/db* mice

Next, we examined whether lipids accumulated in the thyroid follicular cells of *ob/ob* and *db/db* mice. We could not detect TS in the thyroid tissue of *ob/+* mice age 6 and 13 weeks (Figure 5A). By contrast, TS was clearly observed in *ob/ob* mice age 6 and 13 weeks (Figure 5A). Notably, a higher proportion of lipid droplets was observed in 13-week-old than in 6-week-old *ob/ob* mice (Figure 5A). In addition, we found that the area occupied by IFA depots in the thyroid tissues of *ob/ob* mice age 6 weeks (*ob/+* vs *ob/ob*; 4 ± 0.63% vs 28.7 ± 3.6%, $P < .010$) and 13 weeks (*ob/+* vs *ob/ob*; 12.3 ± 2.34% vs 33.1 ± 1.8%, $P <$

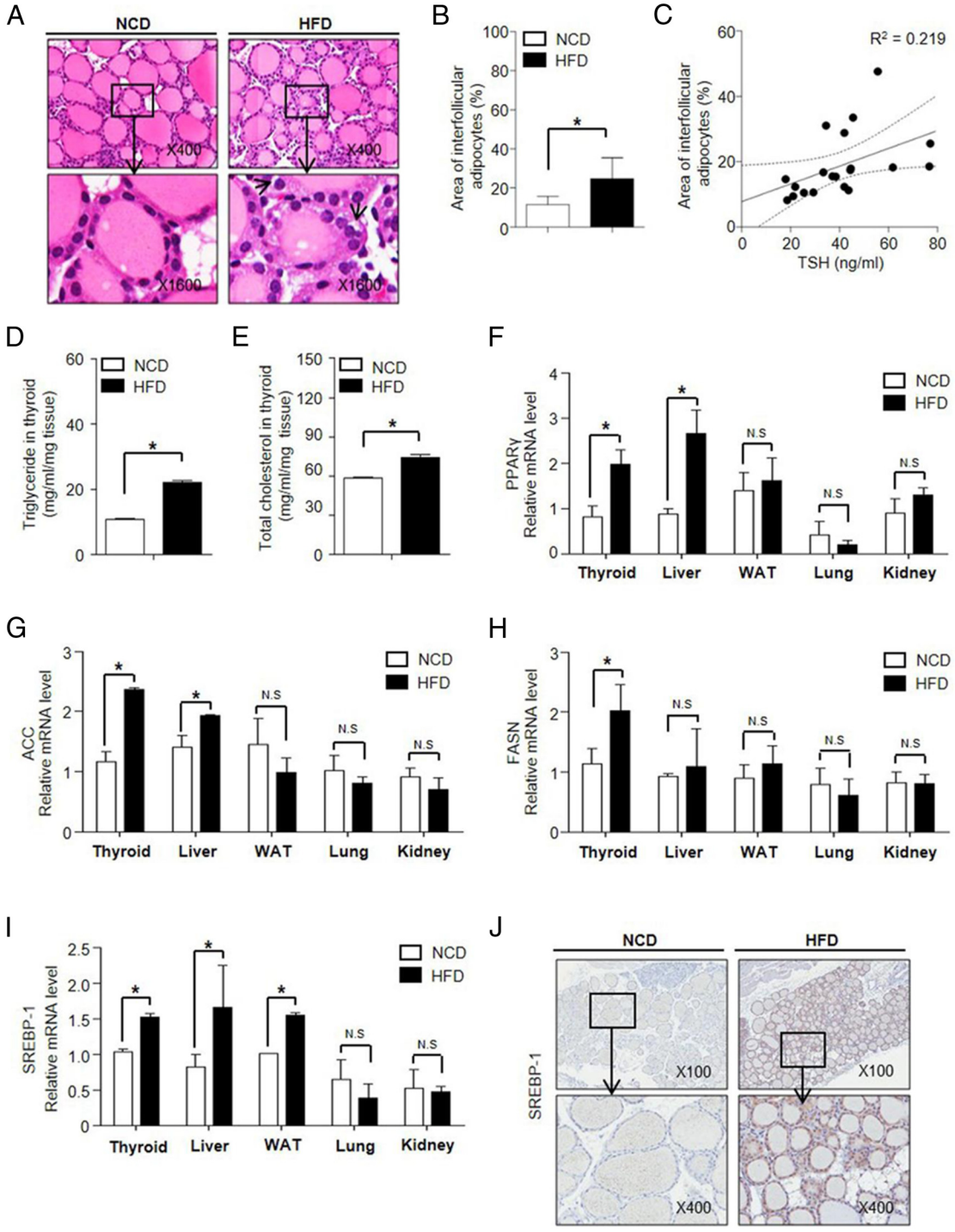

Figure 3. Lipogenesis and steatosis in the thyroid gland of mice with diet-induced obesity. A, Representative microphotographs of H&E paraffin sections of thyroid tissue taken from NCD- or HFD-fed mice for 8 weeks (n = 10 per group). Steatosis (lipid droplets) in thyroid follicular cells was seen in thyroid sections from HFD-fed mice (arrow). B, The adipocyte area was measured in paraffin sections of thyroid tissue taken from NCD- or HFD-fed mice for 8 weeks. C, The Pearson correlation coefficiency was calculated to a percentage differential between the serum TSH level and IFA depots (solid line; R^2) coefficient of determination, dotted line; 95% of R^2 coefficient of determination.) D and E, Tissue TG and cholesterol levels were measured to quantify lipid concentration in the thyroid of NCD- (open bars) and HFD-fed (filled bars) mice. F–I, Relative mRNA levels of lipogenic genes, such as PPARγ, ACC, FASN, and SREBP-1, in NCD- or HFD-fed mice for 8 weeks were measured. mRNAs obtained from the thyroid, liver, white adipose tissue, lung, and kidney were analyzed by RT-qPCR, and then normalized to the expression of 18S rRNA. J, Representative microphotographs of thyroid tissues from NCD- and HFD-fed mice immunostained for the expression of SREBP-1 are shown. SREBP-1 relative mRNA expression was higher in the nucleus and cytoplasm of thyroid follicular cells of HFD-fed mice than in those of NCD-fed mice. Values are means ± SD; *, $P < .05$; N.S., not significant.

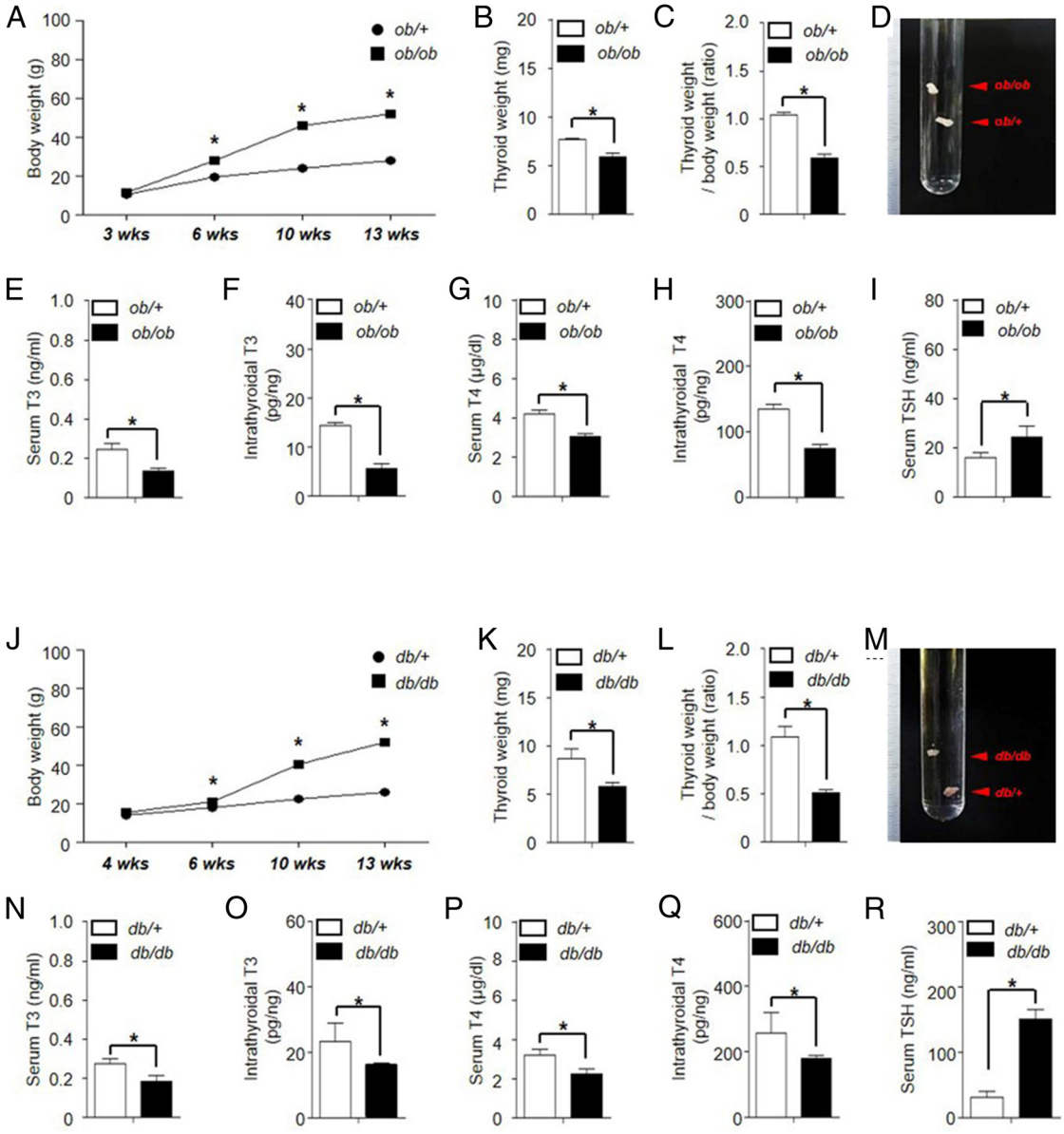

Figure 4. Thyroid dysfunction in genetically obese mice. A, Changes in body weights of *ob*/+ and *ob*/*ob* mice (n = 6 per group) are shown. B and C, The thyroid weight (B) and the thyroid-weight-to-body-weight ratio (C) were measured in *ob*/+ and *ob*/*ob* mice as indicated. D, The specific gravities of the thyroids in *ob*/+ and *ob*/*ob* mice were examined using a serial dilution of glycerol. E–I, Serum T_3 (E), T_4 (G), and TSH (I) levels (n = 10 per group), and intrathyroidal T_3 (F) and T_4 (H) levels (n = 4 per group) were measured in age-matched control mice. J, The changes in body weight in *db*/+ and *db*/*db* mice relative to control mice (n = 6 per group) are shown. K and L, The thyroid weight (K) and the thyroid-weight-to-body-weight ratio (L) were measured in *db*/+ and *db*/*db* mice. M, The specific gravities of the thyroids of *db*/+ and *db*/*db* mice were examined as in panel D. N–R, Serum T_3 (N), T_4 (P), and TSH (R) levels (n = 10 per group), and intrathyroidal T_3 (O) and intrathyroidal T_4 (Q) (n = 4 per group) were measured in age-matched control mice. Values are means ± SD; *, $P < .05$; N.S., not significant.

.001) was larger than that of age-matched *ob*/+ mice (Figure 5B). Transmission EM examination showed multiple cytoplasmic lipid droplets in the thyroid follicular cells of both *ob*/*ob* and *db*/*db* mice (Figure 5, C and F). TS was detected in *db*/*db* mice as shown in *ob*/*ob* mice (Figure 5, D and F). The area occupied by IFA in *db*/*db* mice age 6 weeks (*db*/+ vs *db*/*db*; 9.5 ± 0.8% vs 51.3 ± 2.3%, $P < .002$) and 13 weeks (*db*/+ vs *db*/*db*; 10.6 ± 0.8% vs 31.6 ± 2.4%, $P < .002$) was larger than that in age-matched *db*/+ mice (Figure 5E). Thyroid follicular cells are tightly surrounded with capillary structures (angiofollicular units), which serve for hormone transport (25). To examine whether lipid accumulation in thyroid follicular cells affects the structural integrity of angiofollicular units in the thyroid gland of *ob*/*ob* and *db*/*db* mice, we performed immunohistochemistry staining for CD31, an endothelial cell marker. The staining intensity of CD31 was significantly less intense in the thyroid tissue of *ob*/*ob* mice age

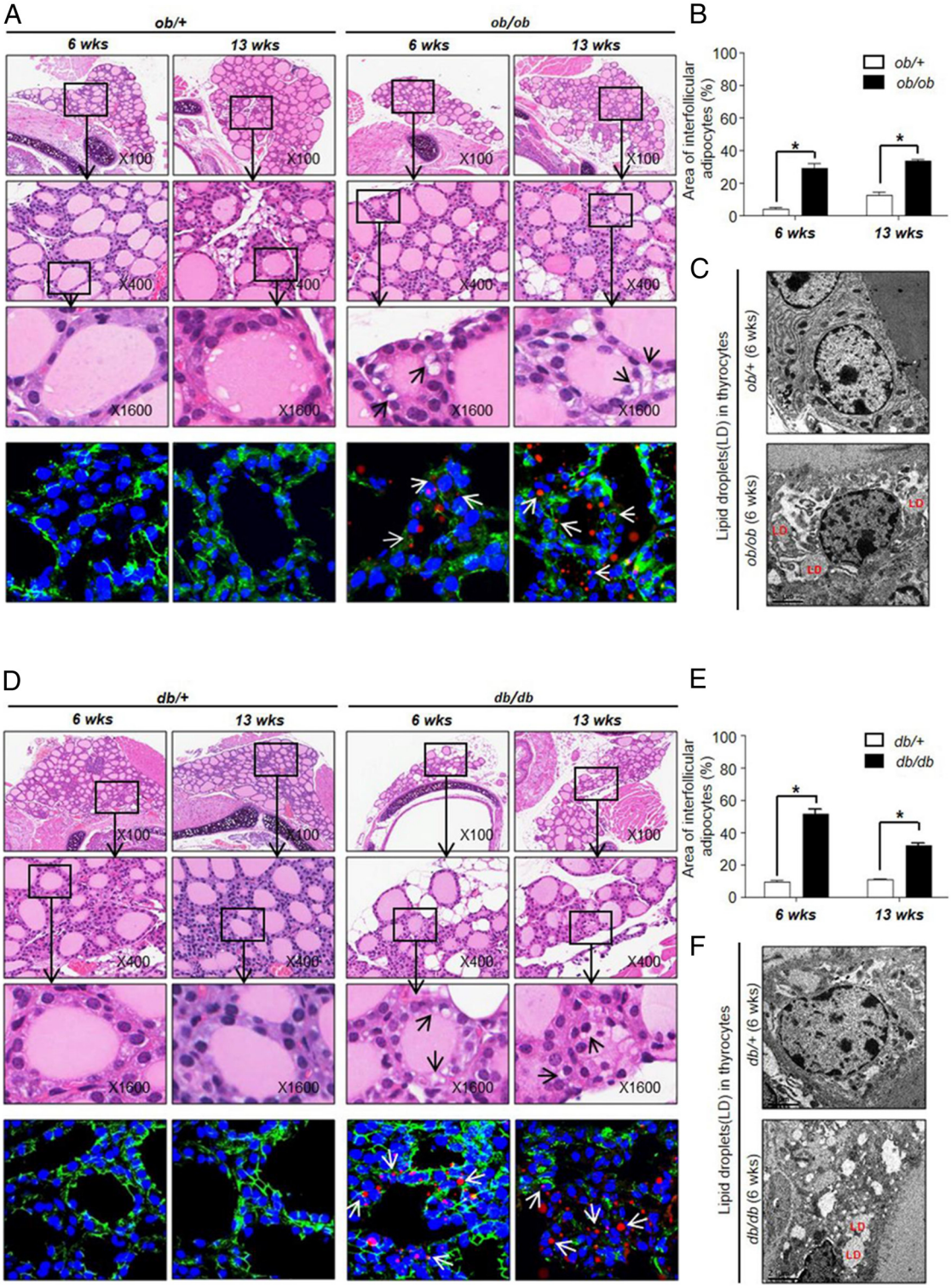

Figure 5. Lipogenesis and steatosis in genetically obese mice. A, Top: Microphotographs of H&E sections of thyroid tissues taken from 6- and 13-week-old *ob*/+ and *ob*/*ob* mice (n = 6 per group) are shown. Representative higher magnification images of follicle and thyroid follicular cells in the thyroid gland of mice are displayed. An arrow indicates lipid droplets (TS). Bottom: Thyroid follicular cells were stained with anti-β catenin antibody (green), BODIPY (red), and DAPI (blue). TS was observed in 6- and 13-week-old *ob*/*ob* mice (Arrow) B, The area of interfollicular adipocytes was measured in thyroid tissue from *ob*/+ (open bars) and *ob*/*ob* (filled bars) mice. C, Lipid droplets in thyroid follicular cells were observed in *ob*/*ob* mice using EM. D, Top: Representative images of H&E-stained thyroid sections and higher magnification images of follicle and thyroid follicular cells in *db*/+ and *db*/*db* mice are shown. Bottom: Triple staining with anti-β catenin antibody (green), BODIPY (red), and DAPI (blue) was performed in thyroid tissue. Arrow indicates TS (n = 6 per group). E, The area of interfollicular adipocytes of *db*/+ (open bars) and *db*/*db* (filled bars) mice was measured as in (B). F, Lipid droplets in thyroid follicular cells were observed in *db*/*db* mice using EM. Values are means ± SD; *, $P < .05$; N.S., not significant.

6 weeks (5.6 ± 0.4 mm^3, $P < .003$) and 13 weeks (8.4 ± 2.8 mm^3, $P < .01$) than in that of age-matched *ob*/+ mice (6 and 13 wk; 15 ± 1.6 mm^3 and 17.4 ± 2.1 mm^3, respectively) (Supplemental Figure 5, A and B). The thyroid follicular cells in *ob*/+ and *db*/+ mice contained normal-shaped mitochondria and ER (Supplemental Figure 6, A and C). In contrast, the thyroid follicular cells in *ob/ob* and *db/db* mice had indented or enlarged nuclei, normal-shaped mitochondria, lipid droplets, and a markedly distended ER (Supplemental Figure 6, B and D). TS and expansion of IFA depots were significantly more prominent in severe obesity mouse models, *ob/ob* and *db/db* mice. In addition, TS was associated with structural abnormalities of cellular organelles; in particular, the ER lumen was dilated (Supplemental Figure 6, B and D) and defects were observed in angiofollicular structures (Supplemental Figure 5, A and B). Both the ER lumen and angiofollicular structures are critical for thyroglobulin synthesis and hormone transport. These observations suggest that structural defects in cellular organelles and angiofollicular units might be the underlying cause of thyroid dysfunction observed in genetically obese mice.

Administration of PPARγ agonist did not improve TS in *ob/ob* and *db/db* mice

Previous studies suggested that the nonadipose PPARγ receptor is critically involved in lipogenesis and lipid accumulation in the liver and muscle and its expression is observed in thyroid cells (26). To examine whether administration of a PPARγ agonist, such as RGZ, modifies lipid accumulation or improves thyroid dysfunction, we treated *ob/ob* and *db/db* mice with RGZ for 3 weeks (Supplemental Figure 7). RGZ-treated *ob/ob* mice showed a significantly smaller thyroid weight (vehicle vs RGZ; 7 ± 0.2 mg vs 6 ± 0.5 mg, $P < .002$) and thyroid-weight-to-body-weight ratio (vehicle vs RGZ; 1 ± 0.02 vs 0.9 ± 0.02, $P < .029$) than vehicle-treated *ob/ob* mice (Supplemental Figure 7, A–D). The weight of various tissues except the liver and muscle was significantly different in RGZ-treated *ob/ob* mice; however, the tissue-weight-to-body-weight ratio of only three tissues, which were liver, sc white adipose tissue, and muscle, showed a critical distinction between the two groups (Supplemental Figure 7, E and F). TS did not differ significantly between the vehicle-treated *ob/ob* and RGZ-treated *ob/ob* mice (Figure 6A). However, IFA was significantly higher in RGZ-treated *ob/ob* mice than in vehicle-treated *ob/ob* mice (vehicle vs RGZ; 26.2 ± 3.2% vs 38 ± 4.2%, $P < .014$) (Figure 6B; Supplemental Figure 7, G–K).

Moreover, TS (Figure 6C) or IFA areas (Figure 6D) in RGZ-treated *db/db* mice was not significantly different from that in vehicle-treated *db/db* mice. Overall, these findings suggest that RGZ administration did not significantly modify established follicular cell steatosis in the thyroid glands of *ob/ob* and *db/db* mice. TSH levels (vehicle vs RGZ; 49.28 ± 7 ng/mL vs 32.2 ± 2.8 ng/mL, $P < .016$) were significantly lower in RGZ-treated *db/db* mice, but were unaffected in RGZ-treated *ob/ob* mice (Figure 6, E and F). RGZ treatment partially improved thyroid dysfunction in *db/db* mice, as shown by the lower serum TSH levels.

Discussion

Recently, it was demonstrated that ectopic fat accumulation causes organ dysfunction (3, 13, 27). However, thyroid dysfunction in the context of obesity has not been thoroughly investigated. Here, we revealed the morphological changes that take place in the thyroid gland in obese humans and obese animal models, namely, DIO, *ob/ob*, and *db/db* mice. Detailed examination of human thyroid lobes obtained from the contralateral side of obese euthyroid patients with papillary microcarcinoma showed two prominent features, namely, an expansion of IFA depots and TS. Adipose tissue produces and releases a variety of secretory factors, including adipokines; leptin, adiponectin, and resistin, as well as cytokines and chemokines (28). It is conceivable that these secretory factors act as active paracrine factors in the regulation of thyroid function in obese patients.

In this study, thyroid steatosis in the context of obesity may directly affect the hormone synthesis capacity of thyroid cells because thyroglobulin processing is affected by ER dysfunction, a feature usually observed in conditions of excessive intracellular lipid accumulation (29, 30). The rodent models of obesity used in this study showed variable degrees of thyroid dysfunction. Thyroid hormone and TSH levels in DIO mice are characteristic of primary thyroid dysfunction (9, 31). The genetically obese mice, namely *ob/ob* and *db/db* mice, had lower intrathyroidal T_3 and T_4 levels, suggesting decreased synthesis capacity in the thyroid gland of these mice models. It is well known that leptin modulates the hypothalamo-pituitary-thyroid axis. However, both *ob/ob* and *db/db* mice consistently showed evidence of primary thyroid failure. Serum T_3 levels are affected by thyroid gland secretory activities and the conversion of T_4 by deiodinase in peripheral tissues including adipose tissue (31, 32). Deiodinase activity in adipose tissue may compensate for thyroid secretory dysfunction to balance the systemic effects of thyroid hormones in *ob/ob* and *db/db* mice. Based on the observed

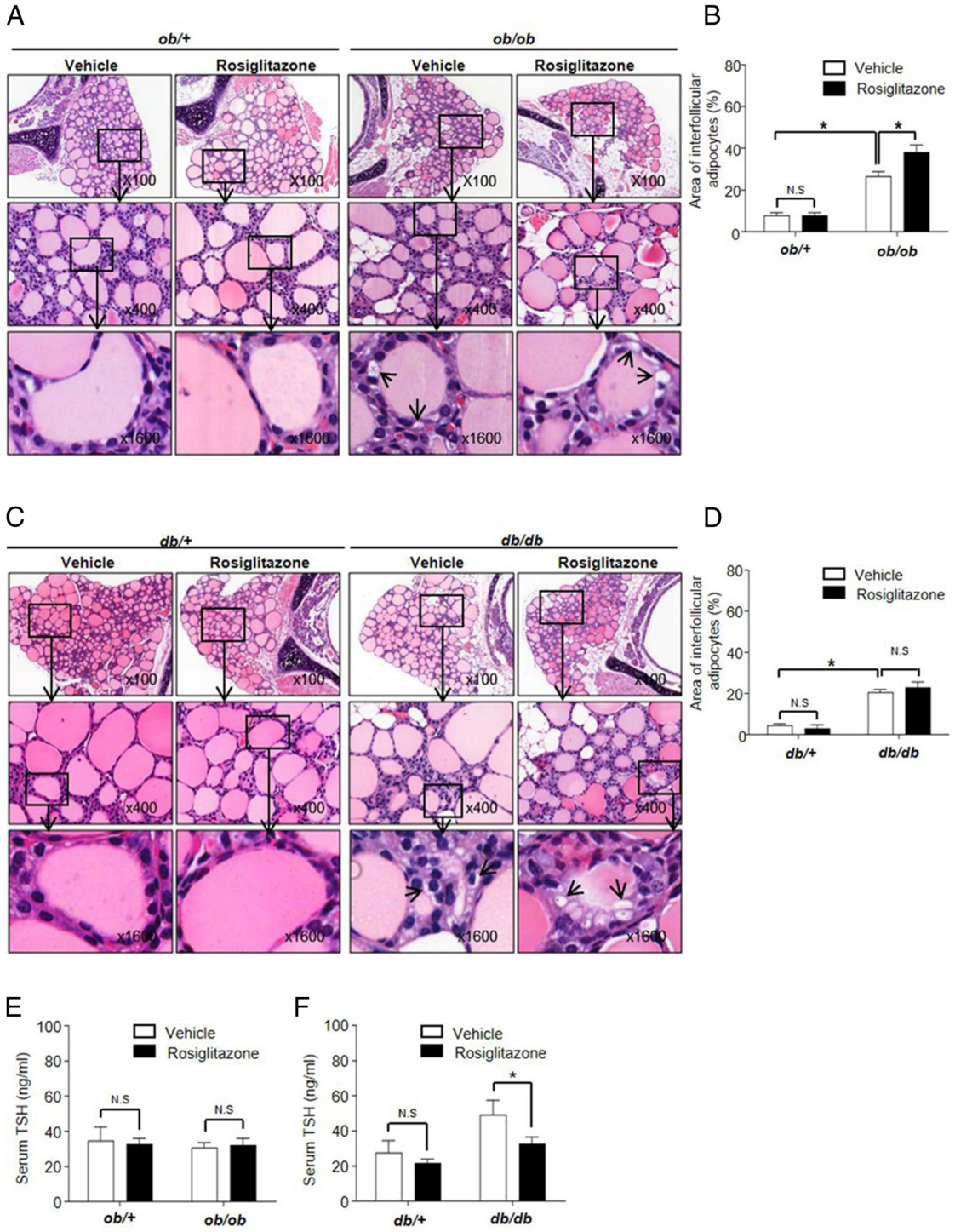

Figure 6. Effect of RGZ administration on thyroid follicular cell steatosis. Six week-old *ob/ob* and *db/db* mice, and their age-matched controls (*ob/+* and *db/+*) were treated with vehicle or RGZ (4 mg/kg/d; n = 5 per group) for 3 weeks. A, Representative microphotographs of H&E-stained thyroid sections from 9-week-old *ob/+* and *ob/ob* mice are shown. Higher magnification images of the boxed parts indicate TS (Arrows). B, The adipocyte area was measured in paraffin sections of thyroid tissue taken from vehicle- or RGZ-treated *ob/+* and *ob/ob* mice. C, Representative microphotographs of H&E-stained thyroid sections from *db/+* and *db/db* mice are shown. Arrow suggests TS. D, The adipocyte area was measured in paraffin sections of thyroid tissue taken from vehicle- or RGZ-treated *db/+* and *db/db* mice. E and F, Serum TSH levels were measured in vehicle or RGZ-treated mice. Values are means ± SD; *, $P < .05$; N.S., not significant.

thyroid hormone and TSH levels, we propose that rodent models of obesity present mild thyroid dysfunction reminiscent of primary hypothyroidism in humans.

It is interesting that *db/db* mice showed increased levels of TSH compared with *ob/ob* mice and HFD-fed mice. Common phenotypic features mostly overlapped between

db/db and *ob/ob* mice, but they displayed characteristic features in endocrine and metabolic regulation. It has been reported that *ob/ob* and *db/db* mice have reduced levels of brain T_4 content compared with control mice. Furthermore, the content of brain T_4 in *db/db* mice was less than that of *ob/ob* mice (brain T_4 *ob/ob* vs *db/db*; 522 ± 167 pg/organ vs 280 ± 28 pg/organ) (33). Attenuation of negative feedback by reduced tissue content of thyroid hormones in *db/db* mice may affect the setting of the TRH-TSH axis that maintains a higher TSH level compared with *ob/ob* mice. Multiple cytokines and growth factors are known to be involved in the regulation of TRH and TSH secretion in the hypothalamus and pituitary gland. For example, TNF-α, a suppressor of TRH synthesis, was reduced in *db/db* mice compared with *ob/ob* mice (34). Taken together, differential thyroid hormone metabolism in hypothalamic TRH neurons may have primary permissive roles in higher TSH levels in *db/db* mice compared with *ob/ob* mice.

To identify the cause of thyroid dysfunction in DIO mice, we examined the expression of genes that are critical for thyroid hormone synthesis and maintenance of differentiated thyroid gland function. We found that the expression levels of thyroid-specific mRNAs such as TSH receptor, thyroperoxidase, sodium-iodide symporer, and thyroglobulin were increased in the thyroid gland of DIO mice. The uniform increase in the expression of these genes may result from the stimulatory actions of up-regulated TSH (35). Therefore, primary thyroid dysfunction in DIO mice may not be caused by defects in thyroid-specific gene expression but by defects in hormone synthesis including thyroglobulin processing.

The thyroid gland of DIO mice showed enhanced expression of SREBP-1, which mediates de novo lipogenesis in hepatic steatosis. Moreover, the expression level of lipogenesis-regulation genes such as SREBP-1, PPARγ, ACC, and FASN was slightly up-regulated in the thyroid of DIO, HFD-fed mice for 8 weeks. These results suggest that the thyroid gland can trigger gene expression programs involved in de novo lipogenesis.

To understand the cause of thyroid dysfunction in genetically obese mice, we examined organelle morphology using transmission EM. Thyroid follicular cells in *ob/ob* and *db/db* mice showed significant swelling of the ER lumen. ER swelling was observed in endocrine cells, such as beta cells, and secretory defects were associated with moderate obesity and diabetes in the mouse models (36, 37). Thyroid cells actively process the thyroglobulin molecule in the ER (38, 39), and defective thyroglobulin processing commonly results in huge thyroid cell dilatation (40, 41). Although the mechanism of ER lumen dilatation in thyroid follicular cells of obese mice is unknown, perturbations in intracellular nutrient and energy fluxes, and severe alterations in tissue architecture may be involved (30). ER dysfunction and subsequent stress responses may result in defective luminal processing and thyroglobulin maturation, ultimately causing defective thyroid hormone synthesis.

The mechanisms by which RGZ regulates steatosis include induced hypolipidemia, enhanced "de novo" fatty acid synthesis, decreased biosynthesis of lipids within the peroxisome, substantially altered free fatty acid metabolism in the heart, and an unusual accumulation of polyunsaturated fatty acids within adipose tissue (42). However, the effects of RGZ in the thyroid have only been demonstrated in thyroid cancer and include induced radioiodine uptake and reduced serum thyroglobulin levels (43, 44). In the present study, RGZ treatment of *ob/ob* mice improved glucose disposal, decreased thyroid weight, and increased IFA and sc fat deposition. However, steatosis in thyroid follicular cells did not improve following RGZ treatment. The effect of RGZ was marginal because the expression level of PPARγ was low in the thyroid of lean mice. This result is consistent with the notion that RGZ treatment is insufficient because the expression level of PPARγ is low in the liver of lean mice (42).

In summary, the present findings suggest that IFA, TS, and thyroid dysfunction develop during obesity although we could not identify the mechanism of lipid accumulation in the thyroid gland. Taken together, these data suggest that thyroid dysfunction may be associated with thyroid follicular cell steatosis and interfollicular fat accumulation.

Acknowledgments

Address all correspondence and requests for reprints to: Minho Shong, MD, PhD, Research Center for Endocrine and Metabolic disease, Chungnam National University School of Medicine, 33 Munhwa-ro, Junggu, Daejeon 301-721 Korea. E-mail: minhos@cnu.ac.kr.

This work was supported by the Basic Science Research Program of the National Research Foundation of Korea, funded by the Ministry of Education, Science and Technology (2012R1A2A1A03002833), Sejong, Korea.

The funders played no role in formulating the study design, collecting data and analysis, deciding to publish, or in preparing the manuscript.

Disclosure Summary: The authors have nothing to disclose.

References

1. **Singer SJ, Nicolson GL.** The fluid mosaic model of the structure of cell membranes. *Science*. 1972;175(4023):720–731.
2. **Chen X, Iqbal N, Boden G.** The effects of free fatty acids on gluco-

neogenesis and glycogenolysis in normal subjects. *J Clin Invest*. 1999;103(3):365–372.
3. **Unger RH.** Lipid overload and overflow: Metabolic trauma and the metabolic syndrome. *Trends Endocrinol Metab*. 2003;14(9):398–403.
4. **Yang H, Galea A, Sytnyk V, Crossley M.** Controlling the size of lipid droplets: Lipid and protein factors. *Curr Opin Cell Biol*. 2012;24(4):509–516.
5. **So JS, Hur KY, Tarrio M, et al.** Silencing of lipid metabolism genes through IRE1α-mediated mRNA decay lowers plasma lipids in mice. *Cell Metab*. 2012;16(4):487–499.
6. **Li JZ, Ye J, Xue B, et al.** Cideb regulates diet-induced obesity, liver steatosis, and insulin sensitivity by controlling lipogenesis and fatty acid oxidation. *Diabetes*. 2007;56(10):2523–2532.
7. **Unger RH.** Lipotoxic diseases. *Annu Rev Med*. 2002;53:319–336.
8. **Thvilum M, Brandt F, Brix TH, Hegedüs L.** A review of the evidence for and against increased mortality in hypothyroidism. *Nat Rev Endocrinol*. 2012;8(7):417–424.
9. **Reinehr T.** Obesity and thyroid function. *Mol Cell Endocrinol*. 2010;316(2):165–171.
10. **Bjorntorp P.** Endocrine abnormalities of obesity. *Metabolism*. 1995;44(9 Suppl 3):21–23.
11. **Asvold BO, Bjøro T, Vatten LJ.** Association of serum TSH with high body mass differs between smokers and never-smokers. *J Clin Endocrinol Metab*. 2009;94(12):5023–5027.
12. **Kok P, Roelfsema F, Langendonk JG, et al.** High circulating thyrotropin levels in obese women are reduced after body weight loss induced by caloric restriction. *J Clin Endocrinol Metab*. 2005;90(8):4659–4663.
13. **Szczepaniak LS, Victor RG, Mathur R, et al.** Pancreatic steatosis and its relationship to β-cell dysfunction in humans: Racial and ethnic variations. *Diabetes Care*. 2012;35(11):2377–2383.
14. **Montanya E, Nacher V, Biarnés M, Soler J.** Linear correlation between beta-cell mass and body weight throughout the lifespan in Lewis rats: Role of beta-cell hyperplasia and hypertrophy. *Diabetes*. 2000;49(8):1341–1346.
15. **Shimabukuro M, Zhou YT, Levi M, Unger RH.** Fatty acid-induced beta cell apoptosis: A link between obesity and diabetes. *Proc Natl Acad Sci U S A*. 1998;95(5):2498–2502.
16. **van der Zijl NJ, Goossens GH, Moors CC, et al.** Ectopic fat storage in the pancreas, liver, and abdominal fat depots: Impact on β-cell function in individuals with impaired glucose metabolism. *J Clin Endocrinol Metab*. 2011;96(2):459–467.
17. **Prentki M, Nolan CJ.** Islet beta cell failure in type 2 diabetes. *J Clin Invest*. 2006;116(7):1802–1812.
18. **Di Scioscio V, Loffreda V, Feraco P, et al.** Diffuse lipomatosis of thyroid gland. *J Clin Endocrinol Metab*. 2008;93(1):8–9.
19. **Huang GW, Li YX, Hu ZL.** Primary myxoid liposarcoma of the thyroid gland. *J Clin Pathol*. 2009;62(11):1037–1038.
20. **Soda G, Baiocchini A, Nardoni S, Bosco D, Melis M.** Benign tumors of heterotopic tissue in the thyroid gland: A report of two cases of lipomatous lesions. *J Exp Clin Cancer Res*. 2000;19(2):245–248.
21. **Rosen ED, Spiegelman BM.** Adipocytes as regulators of energy balance and glucose homeostasis. *Nature*. 2006;444(7121):847–853.
22. **Flier JS, Harris M, Hollenberg AN.** Leptin, nutrition, and the thyroid: the why, the wherefore, and the wiring. *J Clin Invest*. 2000;105(7):859–861.
23. **Horton JD, Goldstein JL, Brown MS.** SREBPs: Activators of the complete program of cholesterol and fatty acid synthesis in the liver. *J Clin Invest*. 2002;109(9):1125–1131.
24. **Li Y, Xu S, Mihaylova MM, et al.** AMPK phosphorylates and inhibits SREBP activity to attenuate hepatic steatosis and atherosclerosis in diet-induced insulin-resistant mice. *Cell Metab*. 2011;13(4):376–388.
25. **Cohen-Lehman J, Dahl P, Danzi S, Klein I.** Effects of amiodarone therapy on thyroid function. *Nat Rev Endocrinol*. 2010;6(1):34–41.
26. **Matsusue K, Kusakabe T, Noguchi T, et al.** Hepatic steatosis in leptin-deficient mice is promoted by the PPARgamma target gene Fsp27. *Cell Metab*. 2008;7(4):302–311.
27. **Britton KA, Fox CS.** Ectopic fat depots and cardiovascular disease. *Circulation*. 2011;124(24):e837–841.
28. **Cohen JC, Horton JD, Hobbs HH.** Human fatty liver disease: Old questions and new insights. *Science*. 2011;332(6037):1519–1523.
29. **Ulianich L, Garbi C, Treglia AS, et al.** ER stress is associated with dedifferentiation and an epithelial-to-mesenchymal transition-like phenotype in PC Cl3 thyroid cells. *J Cell Sci*. 2008;121(Pt 4):477–486.
30. **Ozcan U, Cao Q, Yilmaz E, et al.** Endoplasmic reticulum stress links obesity, insulin action, and type 2 diabetes. *Science*. 2004;306(5695):457–461.
31. **York DA, Otto W, Taylor TG.** Thyroid status of obese (ob/ob) mice and its relationship to adipose tissue metabolism. *Comp Biochem Physiol B*. 1978;59(1):59–65.
32. **De Pergola G, Ciampolillo A, Paolotti S, Trerotoli P, Giorgino R.** Free triiodothyronine and thyroid stimulating hormone are directly associated with waist circumference, independently of insulin resistance, metabolic parameters and blood pressure in overweight and obese women. *Clin Endocrinol (Oxf)*. 2007;67(2):265–269.
33. **Kaplan MM, Young JB.** Abnormal thyroid hormone deiodination in tissues of ob/ob and db/db obese mice. *Endocrinology*. 1987;120(3):886–893.
34. **Sahai A, Malladi P, Pan X, et al.** Obese and diabetic db/db mice develop marked liver fibrosis in a model of nonalcoholic steatohepatitis: Role of short-form leptin receptors and osteopontin. *Am J Physiol Gastrointest Liver Physiol*. 2004;287(5):G1035–1043.
35. **Kohn LD, Kosugi S, Ban T, et al.** Molecular basis for the autoreactivity against thyroid stimulating hormone receptor. *Int Rev Immunol*. 1992;9(2):135–165.
36. **Lemaire K, Schuit F.** Integrating insulin secretion and ER stress in pancreatic β-cells. *Nat Cell Biol*. 2012;14(10):979–981.
37. **Tersey SA, Nishiki Y, Templin AT, et al.** Islet β-cell endoplasmic reticulum stress precedes the onset of type 1 diabetes in the nonobese diabetic mouse model. *Diabetes*. 2012;61(4):818–827.
38. **Kim PS, Arvan P.** Hormonal regulation of thyroglobulin export from the endoplasmic reticulum of cultured thyrocytes. *J Biol Chem*. 1993;268(7):4873–4879.
39. **van de Graaf SA, Ris-Stalpers C, Pauws E, Mendive FM, Targovnik HM, de Vijlder JJ.** Up to date with human thyroglobulin. *J Endocrinol*. 2001;170(2):307–321.
40. **Kim PS, Kwon OY, Arvan P.** An endoplasmic reticulum storage disease causing congenital goiter with hypothyroidism. *J Cell Biol*. 1996;133(3):517–527.
41. **Kim PS, Hossain SA, Park YN, Lee I, Yoo SE, Arvan P.** A single amino acid change in the acetylcholinesterase-like domain of thyroglobulin causes congenital goiter with hypothyroidism in the cog/cog mouse: A model of human endoplasmic reticulum storage diseases. *Proc Natl Acad Sci U S A*. 1998;95(17):9909–9913.
42. **Watkins SM, Reifsnyder PR, Pan HJ, German JB, Leiter EH.** Lipid metabolome-wide effects of the PPARgamma agonist rosiglitazone. *J Lipid Res*. 2002;43(11):1809–1817.
43. **Tepmongkol S, Keelawat S, Honsawek S, Ruangvejvorachai P.** Rosiglitazone effect on radioiodine uptake in thyroid carcinoma patients with high thyroglobulin but negative total body scan: A correlation with the expression of peroxisome proliferator-activated receptor-gamma. *Thyroid*. 2008;18(7):697–704.
44. **Kebebew E, Lindsay S, Clark OH, Woeber KA, Hawkins R, Greenspan FS.** Results of rosiglitazone therapy in patients with thyroglobulin-positive and radioiodine-negative advanced differentiated thyroid cancer. *Thyroid*. 2009;19(9):953–956.